

PAPER • OPEN ACCESS

Energy harvesting using ferroelectric/ferroelastic switching: the effect of pre-poling

To cite this article: Wenbin Kang *et al* 2023 *Smart Mater. Struct.* **32** 085017

View the [article online](#) for updates and enhancements.

You may also like

- [Review of the mechanical and fracture behavior of perovskite lead-free ferroelectrics for actuator applications](#)
Kyle G Webber, Malte Vögler, Neamul H Khansur et al.
- [Static and dynamic strain coupling behaviour of ferroic and multiferroic perovskites from resonant ultrasound spectroscopy](#)
M A Carpenter
- [Domain observation in the visible-light photocatalyst Bi₄NbO₈Br with the layered perovskite structure](#)
Chengchao Zhong, Daichi Mizushima, Kaito Hirata et al.

Energy harvesting using ferroelectric/ferroelastic switching: the effect of pre-poling

Wenbin Kang^{1,2,3,*} , Cameron Cain^{1,3}, Fan Wang² and John E Huber¹ 

¹ Department of Engineering Science, University of Oxford, Parks Road, Oxford OX1 3PJ, United Kingdom

² Physical Intelligence Department, Max Planck Institute for Intelligent Systems, Heisenbergstr. 3, Stuttgart 70569, Germany

E-mail: kang@is.mpg.de

Received 20 April 2023, revised 8 June 2023

Accepted for publication 26 June 2023

Published 5 July 2023



Abstract

Improved power output and energy density have been achieved in piezoelectric transducers by exploiting ferroelectric/ferroelastic switching. However, a problem is that stable working cycles with polarization switching normally cannot be driven by stress alone. This problem has been addressed by using internal bias fields in a partially poled ferroelectric: the material state is engineered such that compressive stress drives ferroelastic switching during mechanical loading, while residual fields restore the polarized state during unloading. However, although this method has been verified, the devices in engineering material states with the best performance have not been explored systematically. In this work, internal bias fields in a partially poled (pre-poled) ferroelectric are used to guide polarization switching, producing an effective energy harvesting cycle. Devices are tested and optimized in the frequency range 1–20 Hz, and the influence of the degree of pre-poling in the fabrication process on energy harvesting performance is explored systematically. It is found that pre-poling the ferroelectric ceramic to about 25% of the fully poled state results in a device that can generate a power density up to about 26 mW cm^{-3} of active material at 20 Hz, an improvement on prior work and an order of magnitude advance over conventional piezoelectrics. However, maximizing the power density can result in residual stresses that risk damage to the device during preparation or in service. The relationship between fabrication success rate and pre-poling level is studied, indicating that greater degrees of pre-poling correlate with higher survival rate. This provides a basis for balancing energy conversion with device robustness.

Keywords: energy harvesting, piezoelectric, ferroelectric, ferroelastic

(Some figures may appear in colour only in the online journal)

³ Wenbin Kang and Cameron Cain have the same contribution to this study.

* Author to whom any correspondence should be addressed.



Original Content from this work may be used under the terms of the [Creative Commons Attribution 4.0 licence](https://creativecommons.org/licenses/by/4.0/). Any further distribution of this work must maintain attribution to the author(s) and the title of the work, journal citation and DOI.

1. Introduction

In recent decades, there has been a significant rise in the use of wireless technology for mobile phones, portable electronics and noticeably in some new areas, such as biomedical implanted devices [1, 2], wireless sensor networks [3, 4], internet of things [5, 6], and wearable technology [7–9]. However, the batteries used in these applications present fundamental engineering challenges around growing power density demands, reliability, and longevity. The requirement for battery replacement and maintenance [10–12], is costly and becomes particularly troublesome for applications in remote locations. In addition, battery producers are expected to suffer material shortages [12] in the next 5–10 years, pushing manufacturers towards technological alternatives.

A potential solution for some of the energy problems of wireless devices is the conversion of ambient waste energy into useful electrical energy, known as energy harvesting. This concept utilises small amounts of energy that would otherwise be wasted [13–15], providing a possible replacement or a sustainable top-up technology for batteries. In the past decade, energy harvesting from many sources has been studied, including thermal [16, 17], mechanical [18, 19], solar [20, 21] and radio-frequency electromagnetic [22, 23] energy.

Harvesting of mechanical energy [24, 25] has been achieved using piezoelectricity [26–28], electromagnetism [29, 30] and electrostatics [31, 32]. Piezoelectric energy harvesters (PEHs) with high electromechanical coupling have been most widely studied due to the advantages of simplicity, linearity and efficiency. However, PEHs commonly operate best at resonance frequencies of hundreds of Hz upwards, while practical energy harvesting tasks may demand operating frequencies of 10 Hz or less [28, 33, 34]. Although work is being undertaken to widen the bandwidth of low-frequency PEHs [35–38], further work is required to improve performance.

In low-frequency environments (1–20 Hz) typical piezoelectric cantilever energy harvesters generate between 1 and $10 \mu\text{W cm}^{-3}$ [12, 39]. Approaches to increase the power density have mainly focussed on the use of advanced materials or composites. This includes use of macro-fibre-composites [40], nanowire-enabled generators [41], porous cellulose nanofibrous films [42] and a vitamin B_2 -assisted polyvinylidene difluoride (PVDF) [43]. The related technology of triboelectric nanogenerators combines higher power density with great flexibility [44, 45] and has achieved power density over 0.1 mW cm^{-3} at 1 Hz [46].

While many PEHs use ferroelectric materials [47–49], they are typically used in a linear regime of material behaviour, and do not exploit ferroelectric/ferroelastic switching directly. Exploiting non-linear switching has the potential for significantly greater energy density, but may cause fatigue degradation, and presents the challenge of how to design a stable electrical switching cycle driven by stress. Several theoretical designs have been proposed [50–58], but not proven experimentally. Recently, Kang *et al* [59–61] presented an energy harvester in a partially polarized state that overcomes some of the problems. Careful control of the degree of partial poling

(called ‘pre-poling’ in this work) results in an energy harvester that undergoes strong non-linearity during mechanical loading, indicating that switching occurs. However, the device returns to its initial state when unloaded, allowing the energy harvester to work in a purely compressive mechanical loading cycle, with improved fatigue resistance.

Building on the work of Kang *et al* [59–61], the present study systematically explores the effects of pre-poling on energy harvesting performance. Previous work showed that reduction in the degree of pre-poling to about 30% of the polarization in the fully poled state gave rise to good energy density. However, the optimal engineering material state for the energy harvesting devices, as well as the relationship between the fabrication success and prepoling state, have not been studied in previous literature. Here, careful control of the pre-poling process is used to fabricate devices with pre-poling in the range 20%–40% and compare their robustness and energy harvesting performance at 1–20 Hz. It is found that, while reducing the degree of pre-poling generally improves the energy harvesting cycle, this also makes the devices less robust and so more liable to fail during manufacture or through fatigue.

2. Device preparation and experimental set-up

The detailed working mechanism and energy harvesting concept based on ferroelectric/ferroelastic switching can be found in prior publications [59–61]; here a brief summary is given to provide context. The general arrangement of the energy harvester comprises a thin layer of a ferroelectric material sandwiched between electrodes and adhered to a substrate, see figures 1(a) and (b). Alternate bending and relaxation of the substrate compresses and relaxes the ferroelectric layer, driving the energy harvesting cycle. In this respect, the device is no different from typical bending-beam PEHs. The key difference is in the device preparation. During preparation, an unpolarised bulk ferroelectric ceramic is first subjected to electric field to partially polarize it. The ceramic is then diced to produce partially polarized (pre-poled) wafers. This pre-poled material is then bonded to a stiff substrate. Next, the poling process is completed by applying electric field, but now the substrate constrains the ferroelectric layer and can induce a transverse residual tensile stress in the ferroelectric. To complete the preparation, a few cycles of tensile stress are applied to the ferroelectric layer by bending and relaxing the substrate. The resulting transverse tensile stress induced in the ferroelectric layer causes it to partially depolarize. From this state, cyclic compressive loading of the ferroelectric layer, applied by bending the substrate, drives a working cycle in which the through thickness polarization switches back and forth between partially polarized states. No external electric fields are applied; instead internal bias fields direct the ferroelectric switching. Loading and unloading of the compressive stress during the working cycle can move charges against an external electrical impedance, and electrical work can thus be done. The device can be thought of as a type of PEH in which the material state gives rise to a strongly non-linear response. In a

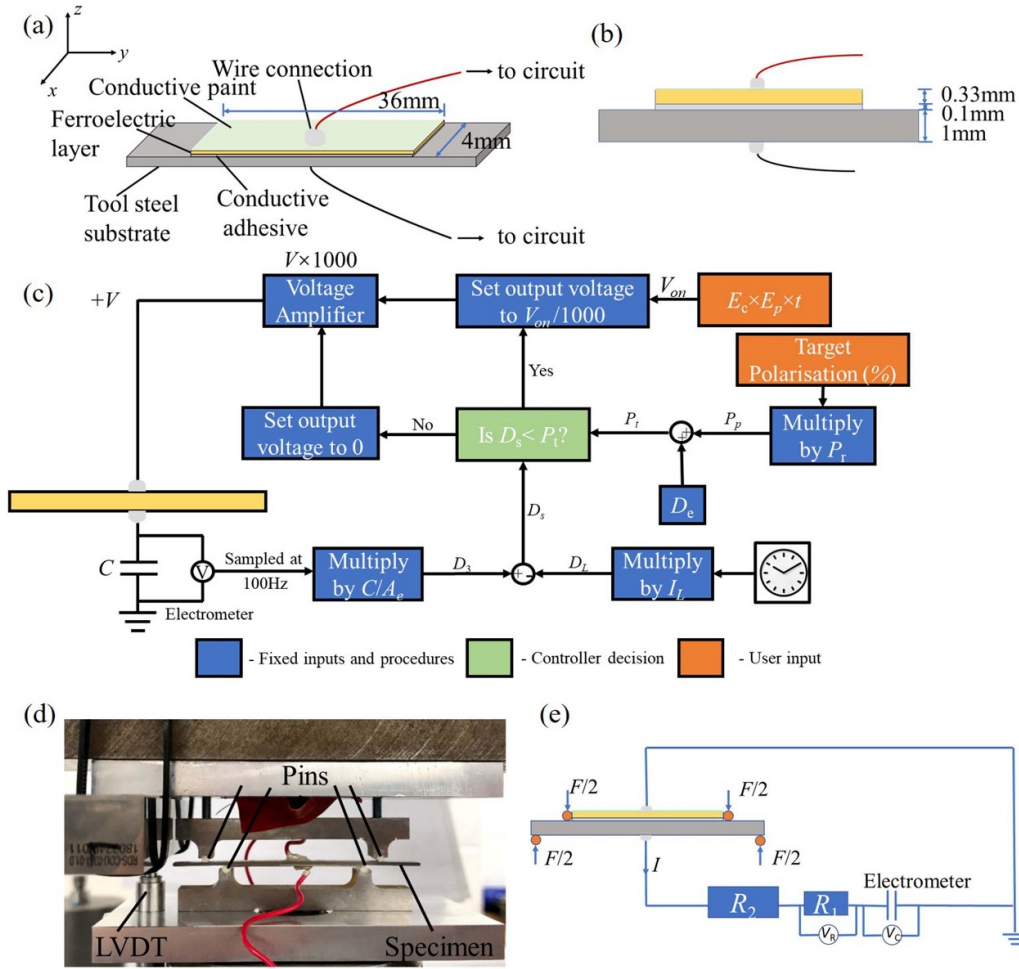


Figure 1. (a) Arrangement of energy harvester. (b) Side view of energy harvester showing layer thicknesses. (c) The control schematic used for both pre-poling and fully poling the ferroelectric. (d) Four-point bending arrangement using a hydraulic test machine for vibrational tests. *Note:* A_e = area of top electrode, D_s = corrected electric displacement of ferroelectric, I_L = known leakage current, P_t = target polarisation, P_r = maximum remnant polarisation, D_e = electric displacement due to linear dielectric effect, E_p applied pre-poling electric field as a fraction of the coercive field.

previous study, the greatest energy output was produced using a 30% pre-poled device, wherein the percentage indicates the degree of poling of the ferroelectric layer, off-substrate, relative to the fully polarized state of the material. This work explores degrees of pre-poling in the range 20%–40% to examine more closely the optimal choice for energy harvesting.

2.1. Device fabrication

Figures 1(a) and (b) shows a device design used in this work. The ferroelectric ceramic utilised is 8/65/35 PLZT (8% Lanthanum doped 65% lead zirconate and 35% lead titanate solid solution). The lanthanum La^{3+} is thought to substitute on Pb^{2+} sites as a donor dopant, resulting in vacancies. This produces soft ferroelectric properties or relaxor behaviour, see [62, 63]. The material was sourced from a standard material supplier. It has a low coercive field ($E_c \approx 0.36 \text{ MV m}^{-1}$) [63, 64] and is mechanically softer than most PZT compositions, which enables easy ferroelastic switching. The ceramic has low porosity and is fine-grained, with approximately $1 \mu\text{m}$

grain size, which can help improve fracture toughness and fatigue resistance. The material has Curie temperature 110°C , and maximum remnant polarization at room temperature of 0.25 C m^{-2} . The device uses a PLZT wafer of dimensions 0.33 mm (thickness) $\times 4 \text{ mm}$ (width) and 36 mm (length), which is adhered centrally to a tool-steel substrate of dimension 1 mm (thickness) $\times 4 \text{ mm}$ (width) and 68 mm (length) using a conductive epoxy layer. The relative thicknesses of the substrate and PLZT wafer reduce non-uniformity of stresses in the PLZT when the substrate is curved. The top electrode is created by using a conductive paint layer across the top surface of the ceramic. This is flexible and has a thickness of about $1 \mu\text{m}$, such that it has a negligible effect on the mechanical loading. Wired connections are made to the top and bottom of the substrate using a conductive epoxy.

An automatic control system was developed to enable accurate and repeatable pre-poling of the ferroelectric. This was achieved by applying an electric field slightly less than the coercive field to induce a gradual poling process, and interrupting this when the target polarization level was

reached. Figure 1(c) shows the control schematic developed for poling, where the state of polarization D_s was continuously estimated by measuring the total charge flow onto the ferroelectric using an electrometer with capacitance C . Care was taken to correct for both the linear dielectric effect and leakage current, both of which were first measured in separate tests [63, 65, 66]. This system was used for both pre-poling of the bulk ceramic (off-substrate) and subsequent full poling (on-substrate). Specifically, the voltage needed for the poling process is generated by the Labview software and NI Instruments device, with a $\times 1000$ voltage amplifier to reach the required electric field. Due to safety conditions set for the voltage amplifier, a safety trip would be activated if V_{on} was applied as a step function. Therefore, the V_{on} is slowly increased over 10 seconds. It was made using a combination of sawtooth and fixed curves with a switching function that activates once the sawtooth reaches its peak value. During poling, if $D_s < P_t$, the required polarisation has not yet been reached so the voltage output is still active to further polarise the electroceramic. When $D_s \geq P_t$, the controller output becomes 0 V and the poling process has been completed. This allowed the ferroelectric ceramics to be pre-poled to the target level with an accuracy within $\pm 0.5\%$. This system was also used in the full-poling process, by setting the electric field to $1.5E_c$ and increasing the target polarisation (P_t) beyond the polarisation saturation limit. Once the polarisation became stable for 30 s, the voltage output was manually switched off. The tensile loading step, which partially depolarizes the ceramic, was applied using a Deben micro-test loading stage, in a four-point bending configuration, as previously reported [59–61].

2.2. Measurement of energy harvesting cycle

A four-point bending test configuration was used to ensure uniformity of the cyclic loading along the length direction of the ferroelectric layer [59–61, 67], see figure 1(d). The bending moment was applied using a servo-controlled hydraulic ram with a 220 N load cell and a displacement transducer, linear variable differential transformer (LVDT). The total applied force F typically followed a sinusoidal waveform with 50 N amplitude, applied to loading pins spaced $a = 5$ mm apart to produce a maximum moment of $(F/2)a = 0.125$ Nm. A 5 N light pre-load was applied to hold the sample in place, with an additional $F = 50$ N cyclic load applied to drive the energy harvesting cycle. The energy harvester developed voltages of order 50 V, that were reduced using a potential divider and logged alongside load, displacement and charge flow data, see figure 1(e). The voltage versus time output of the ferroelectric energy harvester is not sinusoidal because of non-linear switching, but the power output is well approximated by [68]:

$$P = \frac{V_T^2}{(R_1 + R_2)} \quad (1)$$

where V_T is the peak voltage output of the energy harvester and $R_1 + R_2$ is the total resistance of the potential divider. In order to measure performance, a 50 N sinusoidal mechanical loading

cycle was applied at the desired frequency and the system was allowed to stabilize for 20 cycles. Load, displacement, charge and voltage data were logged at 400 Hz sampling rate. Power was calculated using equation (1) with the peak voltage V_T obtained by averaging over 20 cycles.

3. Results and discussion

3.1. Device robustness during fabrication

The device fabrication process included the following stages: 1: pre-poling, 2: material cutting, 3: bonding to substrate, 4: full poling, and 5: mechanical depoling. Stages 2 and 3 are the assembly stages. Due to the requirements of handling delicate wafers of brittle electroceramic material, it was noted that a significant fraction (almost 30%) of wafers failed during assembly. Furthermore, a proportion of wafers failed during stages 4 and 5, see figure 2. The most sensitive part of the process was stage 4 where low levels of pre-poling corresponded to high rates of failure. This can be attributed to the constraint of transverse wafer strain during full poling, leaving the ferroelectric wafer in a state of residual tension. Based on the spontaneous strain $\epsilon_0 \approx 0.385\%$ and Young's modulus $E \approx 68$ GPa of the ceramic, the residual tensile stress may be estimated as [69]:

$$\sigma_1 \approx \frac{1}{3}\epsilon_0(1 - f_p)E \quad (2)$$

where f_p is the pre-polarisation fraction (0 for no pre-poling and 1 for full poling off-substrate). This gives stresses in the range 50–70 MPa for the range of pre-poling explored, with the upper end of the stress range corresponding to 20% pre-poling. Previous studies indicated tensile fracture of 8/65/35 PLZT at about 0.08% strain [70], or 55 MPa tensile stress. This suggests that fracture of the ceramic would become likely during full poling when $f_p < 37\%$, which is reasonably consistent with the findings reported in table 1. Further device failures were noted during stage 5 where additional tensile loading is applied to the wafer to partially depolarize it. These observations indicate that the active material is being subjected to severe loading conditions during fabrication and greater levels of pre-poling are desirable to reduce risk of failure.

3.2. Power performance

Testing of the completed devices was performed using the hydraulic loading rig, as described in section 2.2. Experimentation with different load amplitudes indicated that $F \geq 70$ N caused rapid deterioration with cracks formed in the PLZT wafer, which corresponded to a marked drop in the performance of the ferroelectric energy harvester and the appearance of dark lines in the ceramic when back-lit. By contrast, with 50 N load amplitude, tests could run stably for large numbers of cycles. Previous study [60] suggested that a 30% pre-poled energy harvester outperformed 50%–100% pre-poled devices in terms of power output. Here, closer examination was made of the 20%–40% range of pre-poling at various frequencies.

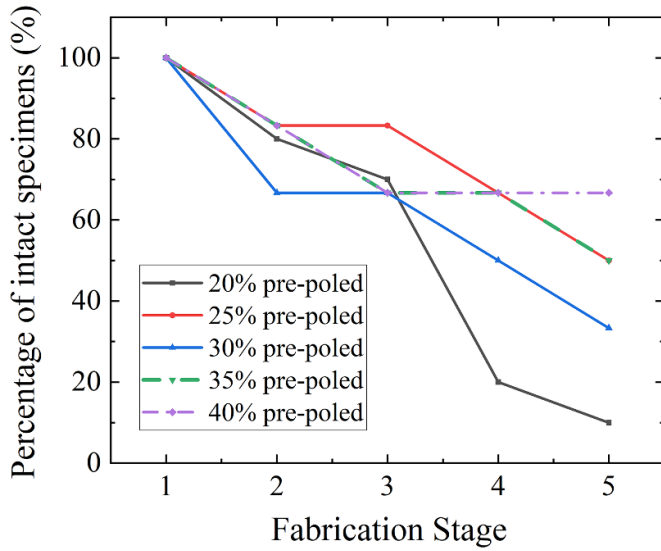


Figure 2. Intact devices after each stage of fabrication.

Table 1. The failure rates of different pre-poling levels.

Pre-polarisation(%)	Assembly failure rate	Full poling failure rate
20	30%	71.4%
25	16.7%	20%
30	33.3%	25%
35	33.3%	0%
40	33.3%	0%

Figure 3 shows the average power output varying with the pre-poling degree and resistive load at 1 Hz, 5 Hz, 10 Hz and 20 Hz. It can be seen that power output generally increases as the pre-poling decreases. This is consistent with the idea that a larger proportion of the ceramic is available for stress-driven domain switching, enabling greater repolarisation of the active material in each cycle. However, the 20% pre-poled device did not follow this trend: observation of the device indicated that multiple cracks formed during cyclic loading in this device, causing performance degradation. It appears that lower levels of pre-poling of the electroceramic require more polarization change in stage 4 of the fabrication process, and the resulting strain changes generate more residual stress. This is more likely to cause device failure during manufacturing or in the working cycle. At the scale of individual grains, domain switching during poling yields a change of inelastic deformation in each grain and associated residual stress, resulting in the formation and evolution of damage and microcracks. The microcracks can extend rapidly during subsequent mechanical or electrical cycling, causing degradation of the electromechanical properties [71, 72]. Degradation of the device is thus an interesting and essential area of further study. It may be speculated that a ferroelectric material with increased strain to failure or fracture toughness could be used advantageously at low pre-poling levels, suggesting ferroelectric composites as a potential alternative to monolithic ceramic wafers.

Figure 3 also suggests that there is a frequency dependent optimal load resistance, independent of the pre-poling level. The optimal resistive load matches the electrical circuit CR time constant to the reciprocal of loading frequency. As the least pre-poled specimen that survived cyclic loading, the 25% pre-poled device yielded the greatest power output at all frequency levels; the power density reached a maximum of 26 mW cm^{-3} at 20 Hz with a $514 \text{ M}\Omega$ resistive load, which is a 30% improvement on our previous reported results for ferroelectric/ferroelastic energy harvesters. Besides, the cycle energy density (the amount of energy generated by the energy harvester per unit volume of active material in a working cycle) of the reported method here is about 1.3 mJ cm^{-3} , which is much greater than the traditional high-performance piezoelectric transducers (around $1\text{--}800 \text{ }\mu\text{J cm}^{-3}$) and comparable with high-performance triboelectric nanogenerators (around $50 \text{ }\mu\text{J cm}^{-3}\text{--}2 \text{ mJ cm}^{-3}$) [60]. The results in figure 3(a), at 1 Hz, are relevant to low frequency applications such as energy harvesting from human motion, which primarily lies between 0 and 5 Hz [28].

At low frequency (figure 3(a)) the 25% pre-poled device shows the greatest power output. However, at 20 Hz (figure 3(d)) there is less variation in power output, with similar performance across the 25%–40% pre-poling range. Figure 4 shows the origin of this effect in more detail, with force-electric displacement and voltage-electric displacement curves at 1 Hz and 20 Hz. Note that the electric displacement data has an arbitrary offset as only charge flow, not absolute electric displacement, was measured. The force-electric displacement curves show that, although the electric displacement amplitude reduces with frequency, the force-electric displacement curves retain similar shapes. However, comparison of the voltage-electric displacement curves indicate that there is greater increase in voltage amplitude with frequency for the 35% and 40% samples. This makes the power output less strongly dependent on pre-poling at higher frequencies. The results suggest that for low frequency (1 Hz) operation, power output is optimized by choosing the lowest pre-poling level that avoids stress-induced failure. At higher frequencies (20 Hz) the use of higher pre-poling levels such as 40% could provide similar performance but with greater robustness.

3.3. Efficiency of the energy harvester

Alongside power output, efficiency becomes an important metric when the device size or energy source are limited. The net mechanical energy input per cycle W_{m0} can be calculated from the measurements in each cycle using

$$W_{m0} = \oint_{\text{cycle}} F dx \quad (3)$$

where x is the measured displacement of the loading pins in the four-point bending rig under force F . However, an alternative definition of mechanical energy input is often used in assessing efficiency of energy harvesters [73–75]:

$$W_m = \frac{1}{2} k x_{\text{max}}^2 \quad (4)$$

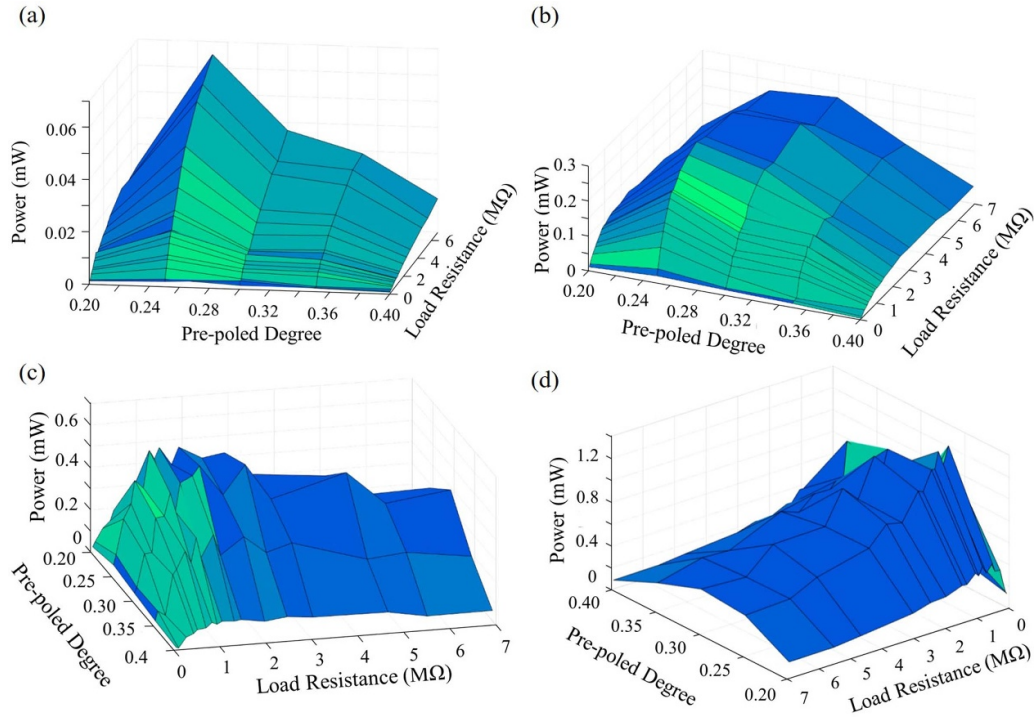


Figure 3. The power output from a ferroelectric/ferroelastic energy harvester, varying with pre-poling degree and load resistance at (a) 1 Hz, (b) 5 Hz, (c) 10 Hz and, (d) 20 Hz.

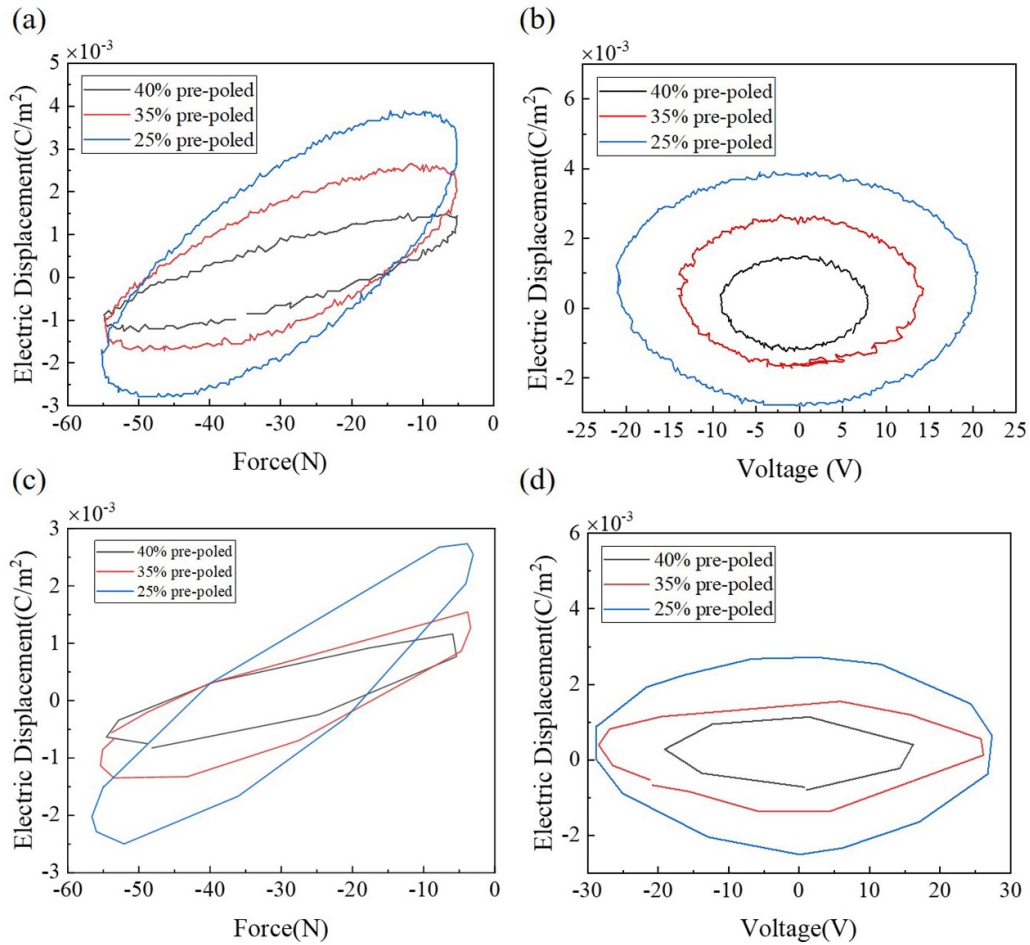


Figure 4. The behaviour different pre-poled devices of the ferroelectric energy harvesters (a) and (b) under 1 Hz of cyclic sinusoidal loading and 6.93 Mω (c) and (d) under 20 Hz of cyclic sinusoidal loading and 942 kω.

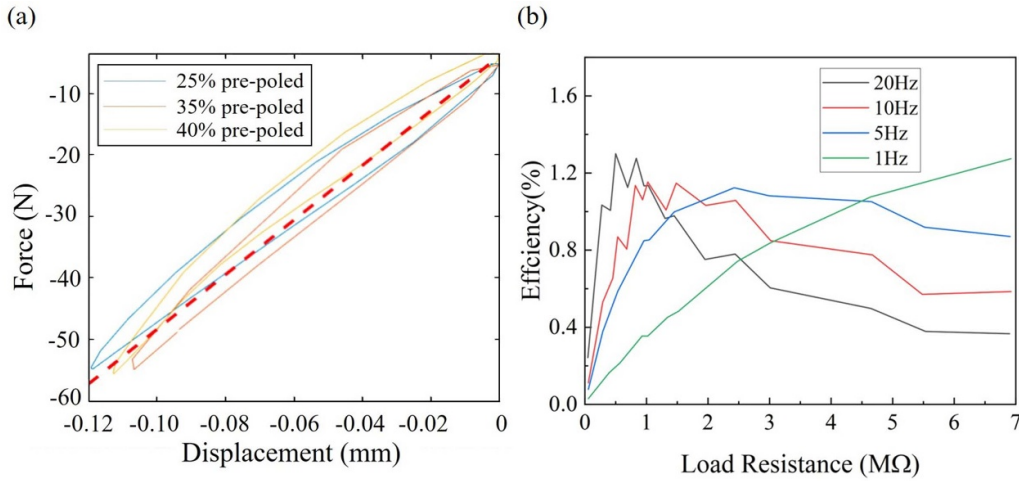


Figure 5. (a) The force F vs pin displacement x response with a fitted (dashed red) line indicating an effective spring constant k . (b) The electromechanical efficiency η_m vs load resistance, at various frequencies, with 25% pre-poling.

where k is the spring constant of the energy harvester and x_{\max} is the maximum displacement of the loading point. It should be noted that, in the current system, $W_m \gg W_{m0}$ as most of the mechanical energy input goes into elastic curvature of the substrate and is released back to the loading system during unloading. This results in low apparent efficiency when equation (4) is used. The difference can be understood from figure 5(a) where W_{m0} is the enclosed area in each hysteresis curve, while W_m is the area between the fitted straight line corresponding to a spring of stiffness k and the x -axis. The spring constant k was estimated at 444 N mm^{-1} by averaging over 30 separate experiments across multiple pre-poled devices and frequencies. For consistency with the piezoelectric energy harvesting literature, calculations were then made using equation (4). The average electrical energy output per cycle at frequency f is estimated, based on equation (1), by [56, 59–61]:

$$W_e = \frac{V_T^2}{2(R_1 + R_2)} \frac{1}{f}. \quad (5)$$

The electromechanical efficiency η_m was then defined as:

$$\eta_m = \frac{W_e}{W_m}. \quad (6)$$

Efficiency data for a 25% pre-poled device is presented in figure 5(b). It can first be noted that the efficiency is extremely low ($<2\%$) which is due to the large amount of stored elastic energy in each cycle. Depending on the application, this energy might be considered ‘wasted’, or returned to the energy source and still ‘available’. Figure 5(b) demonstrates that efficiency can be maximized through external load matching, with the ideal load being frequency dependent. Thus, when the frequency of available mechanical energy is known and fixed, the energy harvester and load can be matched to maximize efficiency. Alternatively, the load can be chosen to minimize sensitivity to the frequency of the energy source.

In practical applications, overloads or uneven loading could alter the engineered state of the energy harvester, resulting

in degradation of performance or damage to the energy harvester. Further testing is needed to establish viable load ranges. However, it is envisaged that a stable operating cycle would be needed to protect the device against such degradation. Thus, there are two main possibilities for application: either (i) the load/displacement cycle should be stable, with the structural design of the device controlling the load seen by the electro-ceramic element to the correct operating range; or (ii) there should be a load-limiting or displacement-limiting element in the load chain, ensuring that the energy harvester does not experience excessive load or displacement. The exact ranges of tolerable load and displacement will depend on the detailed design of the application.

3.4. Power maximization and load matching

It has been demonstrated in section 3.2 that matching the electrical load to the vibration frequency can improve the power output and efficiency of the energy harvester. For load matching, consider the electrical circuit time constant $\tau = R_L C_T$ [76], where R_L is the total load resistance of the external circuit, and C_T is the total capacitance of the circuit, including both the energy harvester itself, and the external capacitance. The capacitance of the energy harvester may be estimated by $\frac{\epsilon_r \epsilon_0 A}{d}$ where ϵ_r is the relative permittivity of the active material, ϵ_0 is the permittivity of free space, A is the area of the capacitor and d is the electrode separation. In this work the energy harvester’s own capacitance is typically small compared to the external capacitance.

Figure 6(a) shows output power versus load resistance data at 20 Hz loading frequency, replotted as output power versus time constant τ . This shows an optimum τ value, for maximum power, that is independent of the degree of pre-poling. It is expected on dimensional grounds that the optimum time constant should be reciprocally related to the mechanical loading frequency, and this is consistent with the data across several experiments, as shown in figure 6(b). This allows load matching for optimum power when the frequency of the mechanical

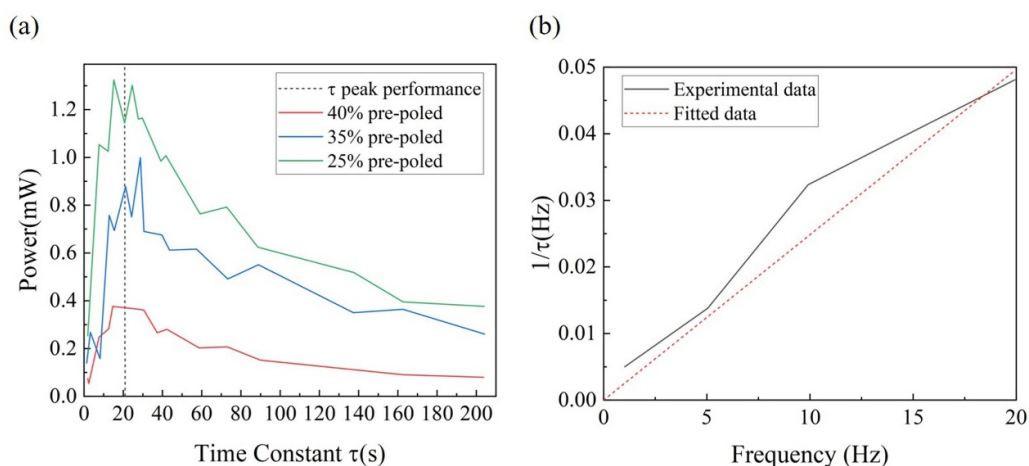


Figure 6. (a) Power output vs circuit time constant for energy harvesters loaded at 20 Hz, indicating optimal time constant. (b) Reciprocal relationship of optimal time constant and mechanical loading frequency.

energy source is well-defined and known. More generally, there is a need to evaluate this energy harvester's performance for non-harmonic loading; given the non-linear nature of the device, this is not readily predicted from harmonic loading data.

4. Conclusions

In this work, the design, fabrication, robustness, and power performance of a ferroelectric/ferroelastic energy harvester was explored. The device design relies on careful pre-poling of an electroceramic, and a system for accurately pre-poling material samples was developed. A relationship between pre-poling level and device robustness was identified, noting that low levels of pre-poling result in higher levels of residual tensile stress. However, low levels of pre-poling were desirable from the point of view of maximizing power density. The resulting compromise between power output and device robustness would be an important factor in practical applications and needs further exploration. Changes to the device design, including the choice of active material and poling process may alleviate this issue.

By varying the pre-poling level and electrical load, a range of device performance was accessed, with a maximum power density of 26 mW cm^{-3} at 20 Hz load frequency and 25% pre-poling. This compares favourably with many energy harvesting technologies, and is an order of magnitude increase relative to typical piezoelectrics. However, the 25% pre-poling level correlated with reduced device robustness, being close to the level at which material cracking occurs during device fabrication. Furthermore, maximum power density was achieved only by matching the electrical time constant and mechanical loading frequency, a step that may not be feasible in practical applications if the loading is non-harmonic or of varying frequency, or if the electrical load is time varying. Thus there are multiple compromises which may only be resolved by application specific designs. Nevertheless, the

results indicate a remarkable increase in cycle energy density relative to well-established PEHs and thus indicate a promising method for high power density energy harvesting at low frequencies.

Data availability statement

All data that support the findings of this study are included within the article (and any supplementary files).

Acknowledgment

The authors gratefully acknowledge support for Wenbin Kang from the Jardine Foundation.

CRediT authorship contribution statement

Wenbin Kang, John Huber: Provided the design for the experiments and implementation steps. **Wenbin Kang, Cameron Cain:** Experimental set-up establishment. **Wenbin Kang, Cameron Cain, Fan Wang:** Fabricated the devices, Measured the output performance and analysed data. **Wenbin Kang, Cameron Cain:** Wrote the manuscript. **Wenbin Kang, Fan Wang, John Huber:** Edited the draft. All authors contributed to the manuscript.

Conflict of interest

The authors declare that they have no known competing financial interests or personal relationships that could have appeared to influence the work reported in this paper.

ORCID iDs

Wenbin Kang  <https://orcid.org/0000-0003-2155-5032>
John E Huber  <https://orcid.org/0000-0003-2375-3673>

References

- [1] Sun M *et al* 2021 Nanogenerator-based devices for biomedical applications *Nano Energy* **89** 106461
- [2] Panda S, Hajra S, Mistewicz K, In-na P, Sahu M, Rajaitha P M and Kim H J 2022 Piezoelectric energy harvesting systems for biomedical applications *Nano Energy* **100** 107514
- [3] Williams A J, Torquato M F, Cameron I M, Fahmy A A and Siens J 2021 Survey of energy harvesting technologies for wireless sensor networks *IEEE Access* **9** 77493–510
- [4] Liu L and Choi S 2021 Miniature microbial solar cells to power wireless sensor networks *Biosens. Bioelectron.* **177** 112970
- [5] Laghari A A, Wu K, Laghari R A, Ali M and Khan A A 2021 A review and state of art of internet of things (IoT) *Arch. Comput. Methods Eng.* **29** 1395–413
- [6] Kumar S, Tiwari P and Zymbler M 2019 Internet of things is a revolutionary approach for future technology enhancement: a review *J. Big Data* **6** 1–21
- [7] Aroganam G, Manivannan N and Harrison D 2019 Review on wearable technology sensors used in consumer sport applications *Sensors* **19** 1983
- [8] Ometov A *et al* 2021 A survey on wearable technology: history, state-of-the-art and current challenges *Comput. Netw.* **193** 108074
- [9] Miller J D, Cabarkapa D, Hermes M J, Fry A C and Berklund C J 2022 Soft magnetic composites as quantitative 3D compression sensors for wearable technology *Adv. Mater. Technol.* **7** 2100784
- [10] Kingsley J 2021 A novel approach using piezoelectricity to power a pacemaker using energy from respiratory motion: breakthrough for a battery free pacemaker *J. Am. Coll. Cardiol.* **77** 3414
- [11] Pan H, Qi L, Zhang Z and Yan J 2021 Kinetic energy harvesting technologies for applications in land transportation: a comprehensive review *Appl. Energy* **286** 116518
- [12] Sezer N and Koç M 2021 A comprehensive review on the state-of-the-art of piezoelectric energy harvesting *Nano Energy* **80** 105567
- [13] Fu H, Mei X, Yurchenko D, Zhou S, Theodossiadis S, Nakano K and Yeatman E M 2021 Rotational energy harvesting for self-powered sensing *Joule* **5** 1074–118
- [14] Zhao X *et al* 2022 A soft magnetoelastic generator for wind-energy harvesting *Adv. Mater.* **34** 2204238
- [15] Ji G and Huber J E 2022 Recent progress in acoustic metamaterials and active piezoelectric acoustic metamaterials-a review *Appl. Mater. Today* **26** 101260
- [16] Yan T, Li T, Xu J, Chao J, Wang R, Aristov Y I, Gordeeva L G, Dutta P and Murthy S S 2021 Ultrahigh-energy-density sorption thermal battery enabled by graphene aerogel-based composite sorbents for thermal energy harvesting from air *ACS Energy Lett.* **6** 1795–802
- [17] Yu C, Kim H, Youn J R and Song Y S 2021 Enhancement of structural stability of graphene aerogel for thermal energy harvesting *ACS Appl. Energy Mater.* **4** 11666–74
- [18] Vijayakanth T, Liptrot D J, Gazit E, Boomishankar R and Bowen C R 2022 Recent advances in organic and organic–inorganic hybrid materials for piezoelectric mechanical energy harvesting *Adv. Funct. Mater.* **32** 2109492
- [19] Long L, Liu W, Wang Z, He W, Li G, Tang Q, Guo H, Pu X, Liu Y and Hu C 2021 High performance floating self-excited sliding triboelectric nanogenerator for micro mechanical energy harvesting *Nat. Commun.* **12** 1–10
- [20] Ahmed S, Li Z, Javed M S and Ma T 2021 A review on the integration of radiative cooling and solar energy harvesting *Mater. Today Energy* **21** 100776
- [21] Zhang Q *et al* 2021 Shadow enhanced self-charging power system for wave and solar energy harvesting from the ocean *Nat. Commun.* **12** 1–11
- [22] Zhu J *et al* 2021 Stretchable wideband dipole antennas and rectennas for RF energy harvesting *Mater. Today Phys.* **18** 100377
- [23] Ullah M A, Keshavarz R, Abolhasan M, Lipman J, Esselle K P and Shariati N 2022 A review on antenna technologies for ambient RF energy harvesting and wireless power transfer: designs, challenges and applications *IEEE Access* **10** 17231–67
- [24] Chalasani S and Conrad J M 2008 A survey of energy harvesting sources for embedded systems *IEEE SoutheastCon 2008 (Huntsville, AL, USA)* (IEEE) pp 442–7
- [25] Maamer B, Boughamoura A, El-Bab A M F, Francis L A and Tounsi F 2019 A review on design improvements and techniques for mechanical energy harvesting using piezoelectric and electromagnetic schemes *Energy Convers. Manage.* **199** 111973
- [26] Kim H S, Kim J-H and Kim J 2011 A review of piezoelectric energy harvesting based on vibration *Int. J. Precis. Eng. Manuf.* **12** 1129–41
- [27] Toprak A and Tigli O 2014 Piezoelectric energy harvesting: state-of-the-art and challenges *Appl. Phys. Rev.* **1** 031104
- [28] Covaci C and Gontean A 2020 Piezoelectric energy harvesting solutions: a review *Sensors* **20** 3512
- [29] Munaz A, Lee B-C and Chung G-S 2013 A study of an electromagnetic energy harvester using multi-pole magnet *Sens. Actuators A* **201** 134–40
- [30] Khalid S, Raouf I, Khan A, Kim N and Kim H S 2019 A review of human-powered energy harvesting for smart electronics: recent progress and challenges *Int. J. Precis. Eng. Manuf. - Green Technol.* **6** 821–51
- [31] Zhang Y, Wang T, Luo A, Hu Y, Li X and Wang F 2018 Micro electrostatic energy harvester with both broad bandwidth and high normalized power density *Appl. Energy* **212** 362–71
- [32] Aljadiri R T, Taha L Y and Ivey P 2017 Electrostatic energy harvesting systems: a better understanding of their sustainability *J. Clean Energy Technol.* **5** 409–16
- [33] Sang C M, Dayou J and Liew W Y 2013 Increasing the output from piezoelectric energy harvester using width-split method with verification *Int. J. Precis. Eng. Manuf.* **14** 2149–55
- [34] Fan K, Tan Q, Liu H, Zhang Y and Cai M 2019 Improved energy harvesting from low-frequency small vibrations through a monostable piezoelectric energy harvester *Mech. Syst. Signal Process.* **117** 594–608
- [35] Dayou J, Liew W and Chow M-S 2012 Increasing the bandwidth of the width-split piezoelectric energy harvester *Microelectron. J.* **43** 484–91
- [36] Leadenham S and Erturk A 2015 Nonlinear m-shaped broadband piezoelectric energy harvester for very low base accelerations: primary and secondary resonances *Smart Mater. Struct.* **24** 055021
- [37] Staaf L, Smith A, Köhler E, Lundgren P, Folkow P and Enoksson P 2018 Achieving increased bandwidth for 4 degree of freedom self-tuning energy harvester *J. Sound Vib.* **420** 165–73
- [38] Dhote S, Yang Z and Zu J 2018 Modeling and experimental parametric study of a tri-leg compliant orthoplanar spring based multi-mode piezoelectric energy harvester *Mech. Syst. Signal Process.* **98** 268–80
- [39] Jin W, Wang Z, Huang H, Hu X, He Y, Li M, Li L, Gao Y, Hu Y and Gu H 2018 High-performance piezoelectric energy harvesting of vertically aligned Pb(Zr,Ti)O₃ nanorod arrays *RSC Adv.* **8** 7422–7
- [40] Khazaei M, Rezaniakolaie A and Rosendahl L 2020 A broadband macro-fiber-composite piezoelectric energy

- harvester for higher energy conversion from practical wideband vibrations *Nano Energy* **76** 104978
- [41] Xu S, Hansen B J and Wang Z L 2010 Piezoelectric-nanowire-enabled power source for driving wireless microelectronics *Nat. Commun.* **1** 1–5
- [42] Zheng Q, Zhang H, Mi H, Cai Z, Ma Z and Gong S 2016 High-performance flexible piezoelectric nanogenerators consisting of porous cellulose nanofibril (CNF)/poly(dimethylsiloxane)(PDMS) aerogel films *Nano Energy* **26** 504–12
- [43] Karan S K *et al* 2019 Designing high energy conversion efficient bio-inspired vitamin assisted single-structured based self-powered piezoelectric/wind/acoustic multi-energy harvester with remarkable power density *Nano Energy* **59** 169–83
- [44] Zhang K, Wang X, Yang Y and Wang Z L 2015 Hybridized electromagnetic–triboelectric nanogenerator for scavenging biomechanical energy for sustainably powering wearable electronics *ACS Nano* **9** 3521–9
- [45] Invernizzi F, Dulio S, Patrini M, Guizzetti G and Mustarelli P 2016 Energy harvesting from human motion: materials and techniques *Chem. Soc. Rev.* **45** 5455–73
- [46] Cao Z, Wu Z, Ding R, Wang S, Chu Y, Xu J, Teng J and Ye X 2022 A compact triboelectric nanogenerator with ultrahigh output energy density of 177.8 J m^{-3} via retarding air breakdown *Nano Energy* **93** 106891
- [47] Dabby N L, Eid F, Elsherbini A A, Lathrop B, Aleksov A and Oster S 2019 Fabric-based piezoelectric energy harvesting *US Patent* 10,215,164
- [48] Yoshimura T, Murakami S, Wakazono K, Kariya K and Fujimura N 2013 Piezoelectric vibrational energy harvester using lead-free ferroelectric BiFeO₃ films *Appl. Phys. Express* **6** 051501
- [49] Lee S K 2013 Energy harvesting electric device *US Patent* 8,373,332
- [50] Münch I, Krauß M, Landis C M and Huber J E 2011 Domain engineered ferroelectric energy harvesters on a substrate *J. Appl. Phys.* **109** 104106
- [51] Münch I, Krauß M, Wagner W and Kamlah M 2012 Ferroelectric nanogenerators coupled to an electric circuit for energy harvesting *Smart Mater. Struct.* **21** 115026
- [52] Patel S, Chauhan A and Vaish R 2014 A technique for giant mechanical energy harvesting using ferroelectric/antiferroelectric materials *J. Appl. Phys.* **115** 084908
- [53] Balakrishna A R and Huber J E 2016 Nanoscale domain patterns and a concept for an energy harvester *Smart Mater. Struct.* **25** 104001
- [54] Wang D, Wang L and Melnik R 2017 Vibration energy harvesting based on stress-induced polarization switching: a phase field approach *Smart Mater. Struct.* **26** 065022
- [55] Wang D, Melnik R and Wang L 2018 Material influence in newly proposed ferroelectric energy harvesters *J. Intell. Mater. Syst. Struct.* **29** 3305–16
- [56] Kang W and Huber J E 2019 Prospects for energy harvesting using ferroelectric/ferroelastic switching *Smart Mater. Struct.* **28** 024002
- [57] Behlen L, Warkentin A and Ricoeur A 2021 Exploiting ferroelectric and ferroelastic effects in piezoelectric energy harvesting: theoretical studies and parameter optimization *Smart Mater. Struct.* **30** 035031
- [58] Warkentin A, Behlen L and Ricoeur A 2023 Model-based investigations of ferroelectric energy harvesting with regard to an improvement of life span and operability *Smart Mater. Struct.* **32** 035028
- [59] Kang W, Chang L and Huber J E 2022 Investigation of mechanical energy harvesting cycles using ferroelectric/ferroelastic switching *Nano Energy* **93** 106862
- [60] Kang W and Huber J E 2022 Energy harvesting based on compressive stress-induced ferroelectric/ferroelastic switching in polycrystalline ferroelectric materials *Cell Rep. Phys. Sci.* **3** 100707
- [61] Kang W, Cain C, Paynter R and Huber J E 2023 A ferroelectric/ferroelastic energy harvester: load impedance and frequency effects *Energy Convers. Manage.* **277** 116687
- [62] Rauls M B, Dong W, Huber J E and Lynch C S 2011 The effect of temperature on the large field electromechanical response of relaxor ferroelectric 8/65/35PLZT *Acta Mater.* **59** 2713–22
- [63] Lynch C S 1996 The effect of uniaxial stress on the electro-mechanical response of 8/ 65/35PLZT *Acta Mater.* **44** 4137–48
- [64] Hwang S, Lynch C and McMeeking R 1995 Ferroelectric/ferroelastic interactions and a polarization switching model *Acta Metall. Mater.* **43** 2073–84
- [65] Hogg M G, Timoshkin I V, Macgregor S J, Wilson M P, Given M J and Wang T 2013 Electrical breakdown of short non-uniform air gaps 2013 19th IEEE Pulsed Power Conf. (PPC) (San Francisco, CA, USA) (IEEE) pp 1–4
- [66] Wöhler F, Muench I and Wagner W 2018 Leakage current and polarization domains in ferroelectric nanogenerators for energy harvesting *Proc. Appl. Math. Mech.* **18** e201800456
- [67] Liu Q, Sadowski A J and Michael Rotter J 2019 Ovalization restraint in four-point bending tests of tubes *J. Eng. Mech.* **145** 04019009
- [68] Junior C D M, Erturk A and Inman D J 2009 An electromechanical finite element model for piezoelectric energy harvester plates *J. Sound Vib.* **327** 9–25
- [69] Huber J E, Fleck N A, Landis C M and McMeeking R M 1999 A constitutive model for ferroelectric polycrystals *J. Mech. Phys. Solids* **47** 1663–97
- [70] Kumar R, Bavbande D, Mishra R, Bafna V, Mohan D and Kothiyal G 2013 Reitveld refinement study of PLZT ceramics *AIP Conf. Proc.* **1512** 620–1
- [71] Kozinov S and Kuna M 2018 Simulation of fatigue damage in ferroelectric polycrystals under mechanical/electrical loading *J. Mech. Phys. Solids* **116** 150–70
- [72] Shieh J, Huber J E and Fleck N A 2006 Fatigue crack growth in ferroelectrics under electrical loading *J. Eur. Ceram. Soc.* **26** 95–109
- [73] Starner T 1996 Human-powered wearable computing *IBM Syst. J.* **35** 618–29
- [74] Starner T and Paradiso J A 2004 Human generated power for mobile electronics *Low Power Electron. Des.* **45** 1–35
- [75] González J L, Rubio A and Moll F 2002 Human powered piezoelectric batteries to supply power to wearable electronic devices *Int. J. Soc. Mater. Eng. Resour.* **10** 34–40
- [76] Hamilton S 2007 *An Analog Electronics Companion: Basic Circuit Design for Engineers and Scientists* (Cambridge University Press)